ELSEVIER

Biophysical Chemistry 73 (1998) 227–239

Biophysical Chemistry

Self-assembly of melanin studied by laser light scattering

Maria Grazia Bridelli*

INFM and Department of Physics, University of Parma, Viale delle Scienze, 43100 Parma, Italy

Received 20 November 1997; received in revised form 24 March 1998; accepted 24 March 1998

Abstract

The unknown molecular weight and chemical structure of melanin place the study of these pigments outside the range of the classical biochemical techniques; thus in this paper the problem of characterizing these heterogeneous biopolymers was approached by means of light scattering techniques, static and dynamic. The static technique allowed us to identify the macromolecular properties ($\langle MW \rangle$ and $\langle R_g^2 \rangle^{1/2}$) of melanin extracted from sepia inksac and of two synthetic analogues: L-Dopa melanin obtained by autooxidation and by enzymatic oxidation by Tyrosinase. By dynamic light scattering (DLS), the hydrodynamic radius R_h was measured to monitor the temporal behaviour of the polymerization and aggregation processes and R_h variation by changing the chemical constraints of the polymerization medium, such as pH and ionic strength. The fractal dimension d of the aggregates of melanin, both natural and synthetic, in the past only recognized during the aggregation of the synthetic one by lowering the pH of the medium, was a useful parameter to further investigate and compare the structure of melanin granules of differing origins, revealing for the natural sample, a structure with clusters that are spherical, not largely hydrated and self-assembled, following a reaction limited aggregation kinetics ($d = 2.38$)

Keywords: Melanin; Light scattering; Polymerization; Hydrodynamic radius; Radius of gyration; Fractal dimension

1. Introduction

Although melanins are a class of pigments widely diffuse in nature, neither their structure nor their function are as yet well understood, despite about three decades of intensive research [1–4].

Melanin, in fact, can be considered as a mixture of more or less similar polymers, apparently made up of different structural units linked through heterogeneous non-hydrolyzable bonds. It is the result of the polymerization of indole-type rings, in both the quinone and hydroquinone oxidation state, randomly crosslinked and staked.

* Fax: +39 521 905223; e-mail: bridelli@vaxpr.pr.infn.it

Abbreviations: DLS, dynamic light scattering; L-Dopa, L-3-[3,4 dihydroxyphenyl]alanine; $\langle MW \rangle$, molecular weight; O.D., optical density; $\langle R_g^2 \rangle^{1/2}$, radius of gyration; R_h, hydrodynamic radius

0301-4622/98/$19.00
PII S0301-4622(98)00148-3

These units represent the product of complex oxidation cycles that start from different precursors and follow various pathways of synthesis, depending on their localization in the organism.

Melanin is distributed throughout both the vegetable and the animal kingdom: it accumulates in living organisms in the form of granules. The complex biosynthetic pathway occurs in vivo in melanocytes, and the process is catalyzed, in the first steps, by a specific enzyme, Tyrosinase, which converts Tyrosine to Dopa and then to Dopaquinone [4,5]. This highly reactive chemical species is subject to oxidative polymerizations, and the polymers that are the product of melanogenesis further aggregate in black-brown granules the size of which is dependent on the localization: in the human body they are responsible for the colour of the skin and hair.

The growth kinetics of the aggregates and the structure of the granules both from natural and synthetic origin have been widely investigated in the last few years [6]. The granule formation process proceeds spontaneously toward the oxidation product and, during the last phases of the in vitro aggregation, it behaves as a 'reversible' process dependent on the pH of the solution, in the sense that low pHs promote aggregation, while the rise of pH toward alkaline values induces the breaking up of the granules in smaller particles. In the absence of any molecular model, this behaviour has been related to the large number of electrical charges carried by the biopolymer. Melanin, in fact, is rich in many ionizable groups such as carboxylic, phenolic and aminic residues, and displays polyanionic properties at physiological pH [7].

Recent studies agree with the hypothesis of the existence of a 'nucleus' in the aggregation of melanin: a small particle of macromolecular or supramolecular size capable of aggregating to build the final structure. The hypothesis was first suggested by Zeise et al. in 1992 [8] as a result of their bio-analytical and SEM studies performed on sepia-inksac melanin. Recently, X-ray diffraction studies on natural (Sepia) and synthetic (from L-Dopa and Tyrosine) melanins have confirmed in both types the presence of a 'fundamental particle' ($r \approx 15$ Å) constituting the building blocks of the melanin granule [9,10].

In the present paper the problem of the structure of the melanin granule was approached by means of light scattering measurements, static and dynamic, to extract complementary information, both structural and concerning the dynamics of aggregation. It is well known that one of the ways to characterize self-association of biological macromolecules is according to the geometry of the final assembled structure which provides suggestions about the mechanisms of formation [11]. In the case of melanin, we found that self-association leads to end structures that can attain very large dimensions, sometimes of the order of microns, frequently of an indefinite degree of polymerization depending on environmental conditions such as pH and ionic strength.

Three different kinds of samples were examined: one natural, extracted from sepia inksac and the other two synthetic, prepared under different conditions of pH and ionic strength and the data were compared.

The persistence over almost two decades of a power law for the mean scattering intensity I vs. q, the Bragg wavevector, confirmed the fractal nature of the aggregates of melanin and allowed us to re-examine, by means of the analysis of the fractal dimension d, the structure of these aggregates.

Huang et al. [12] previously analyzed the dynamics of aggregation of synthetic melanin in aqueous solution (pH 2–3) on the basis of studies on the aggregation of aqueous gold colloids [13], and they detected in the kinetics the sequence of two regimes of aggregation: DLA, (diffusion limited aggregation, in which the particles stick on contact) characterized by clusters with fractal dimension $d = 1.8$, during the first steps of the aggregation processes, and RLA, (reaction limited aggregation, in which the particles stick only after multiple collisions), with aggregates at $d = 2.2$, in the subsequent phases. Here the fractal dimensions detected for synthetic melanin, polymerized under different conditions, and for the natural

one, are discussed with the aim of relating the dynamics of building of the granule with its chemical and physical features in the natural state.

2. Physical principles

The physical parameters associated with the self-assembly process of melanin were extracted by the combined use of light scattering techniques, static and dynamic. It is well known that light which has been scattered by a macromolecular solution contains information about both the static and the dynamic properties of the system under study: static information can be extracted by the intensity and the angular distribution of the scattered light, dynamic information by the spectral analysis of the scattered light.

In the case of solutions of biological macromolecules, the behaviour of the scattered radiation has to be considered in the approximation of large scatterers with respect to wavelength [14]. To yield information about mass and size of macromolecules in solution, scattering intensity can be plotted as in a Zimm plot [15]. Scattered intensities at various concentrations are plotted vs. concentration c and the scattering angle θ as Kc/R_θ, R_θ being the Rayleigh ratio and the optical constant

$$K = \left[2\pi^2 n_0^2 (\mathrm{d}n/\mathrm{d}c)^2\right]/(N_\mathrm{A}\lambda^4) \tag{1}$$

where n_0 is the refraction index of the solvent, $\mathrm{d}n/\mathrm{d}c$ the increment of the refraction index of the solution dependent on the solution concentration, λ the wavelength of the light employed for the experiment and N_A the Avogadro number. By extrapolating the data for $c \to 0$ and $\vartheta \to 0$, the average molecular weight $\langle \mathrm{MW} \rangle$ and the radius of gyration $\langle R_\mathrm{g}^2 \rangle^{1/2}$ can be computed. $\langle R_\mathrm{g}^2 \rangle^{1/2}$ values are independent of the shape of the scatterers. For large scatterers, the interference effect produced by the scattered radiation from different points on the same particle may be described by the function $P(\theta)$, the particle scattering factor. Expressions for $P(\theta)$ for simple geometries are given in the literature [14,16]. We employed for the sphere:

$$P(x) = [(1/x^3)(\sin x - x\cos x)]^2 \tag{2}$$

where $x = q \cdot r$, $q = (4\pi n_0/\lambda)\sin(\theta/2)$ being the scattering wavevector (where n_0 is the refractive index of the solvent) and $r = \sqrt{5/3}\ \langle R_\mathrm{g}^2 \rangle^{1/2}$ the radius of the sphere; for the random coil

$$P(x) = (2/x^2)[\exp(-x) - 1 + x] \tag{3}$$

where $x = q^2 \cdot r^2$, $r = \langle R_\mathrm{g}^2 \rangle^{1/2}$ being the average characteristic radius of the random coil.

As described above, DLS, which yields information concerning the dynamic properties of the system such as diffusion and frictional coefficients, is complementary to the static light scattering technique.

If motion is due to translational Brownian diffusion in a diluted solution of small spherical scatterers, the autocorrelation function is [14,17]

$$g(t) = \exp(-2q^2 Dt) \tag{4}$$

where D is the average diffusion coefficient

$$D = k_\mathrm{B} T/6\pi\eta R_h \tag{5}$$

R_h being the hydrodynamic radius of the spherical macromolecule and η the viscosity coefficient of the solvent.

The theory concerning fractals and the detection of the fractal dimension of a structure has been developed in many books and reviews [18,19]. The more general procedure for determining the fractal dimension of an aggregate uses the approximation following which the intensity of light $I(q)$ scattered by a single particle of radius r_o, for q small compared with $1/r_\mathrm{o}$ but large compared with $1/R_\mathrm{g}$ ($1/R_\mathrm{g} \ll q \ll 1/r_\mathrm{o}$), is

$$I(q) \sim q^{-d} \tag{6}$$

and thus for fractal scatterers the scattered intensity is almost linear on a log-log plot vs. q and the slope is the fractal dimension d.

3. Materials and methods

3.1. Samples: synthetic and natural melanins

Synthetic melanins by autooxidation of L-Dopa (Sigma) were obtained by dissolving L-Dopa up to saturation in salt free aqueous solution buffered (borate buffer 0.1 M) at different pH values (pH 7, 8, 9, 10) and stirred in air for a week. The sample polymerizing at pH 8 was then prepared under different conditions of ionic strength by adding to the starting solutions NaCl in increasing concentrations (0.01, 0.1, 0.5, 1 M).

Melanin by enzymatic oxidation of L-Dopa was synthesized by the action of mushroom tyrosinase (EC 141801) (Sigma) in aqueous solution buffered at pH 7 at the concentration of 8 mg of enzyme per 100 ml of saturated solution of L-Dopa and stirred in air for a week.

The above described method of obtaining melanin from L-Dopa following the two polymerization pathways, by autooxidation and by enzymatic polymerization, is generally accepted by the research community in this field [20].

Samples obtained both by autooxidation and by enzymatic polymerization appeared as black-brown solutions, mixtures in buffer of granules of different average sizes, depending on the pH. After polymerization the melanin solutions were diluted until the best autocorrelation signal was obtained: the dilution was controlled spectrophotometrically in order to maintain O.D.($\lambda = 340$ nm) ≤ 0.2. The samples employed for the analysis of the polymerization kinetics were obtained as diluted solutions of L-Dopa to avoid deeper absorption of light during the last phases of the polymerization process ([L-Dopa] = 0.5 to 1.5×10^{-3} g ml^{-1}).

Natural melanin from sepia ink was an ultrapurified sample, a gift from Dr. Chedekel (Mel-Co, CA, USA): the sample was powdered in a mortar and a weighed portion suspended in aqueous solutions buffered at pH 7.2. The captions of the figures relating to this sample refer in detail to the concentrations employed in the various experiments.

3.2. Light scattering measurements

Light scattering measurements were performed at wavelength $\lambda = 632.8$ nm in a Malvern PCS 100 spectrometer. Cylindrical glass vials (Hellma) with a diameter of 5 mm and height about 10 cm were used as scattering cells and, due to the high difference between the absorbing power of the scattering centers (black melanin granules) and the solvent, no index matching bath was employed. The scattering cells were rinsed extensively in a mixture of alcohol and a concentrated hydrochloric acid solution diluted 1:3 with distilled water. Tridistilled water prefiltered with 0.22-μm Millipore filters was forced through the cell. The water remaining was forced out and the cell was dried by dry nitrogen also prefiltered with a 0.22 μm filter. The cuvettes were closed and so this process excluded dust from the cell.

The apparatus includes a HeNe laser (1.5 mW) and a photomultiplier tube mounted on a rotating arm provided by a goniometer with a vernier scale reading to $1/20°$. The instrument alignment was found to be satisfactory in the angular range $10° \leq \theta \leq 140°$. The optics of the apparatus consists of a focusing system provided with a primary lens on the incoming laser beam and with a Pusey receiver optical system on the scattered beam with a lens with iris f4.5–f16, a rear pinhole and a rotatable turret of apertures controlling the number of coherence areas: the pinhole sizes were varied for different scattering angles by taking into account that typically the scattered light from samples should produce count rates in the range 30 kHz to 150 kHz.

The experimental data were collected at RT and analyzed with a dedicated PC. The correlation computer was used to obtain the autocorrelation function of the photomultiplier current. The technical principles by which our apparatus operated and the details about the combination of hardware and software are well documented elsewhere [21]. The output of the computer gives an exponential curve with a time constant τ related to the half width Γ of the Lorentian line in the corresponding power spectrum according to $1/\tau$

$= \Gamma$. D values were derived from the autocorrelation function $g(t)$ by applying the usual cumulant fit

$$\ln g(t) = C + \Gamma t + \sigma t^2 \quad (7)$$

the first cumulant $\Gamma = (k_B T/6\pi\eta R_h)q^2$ being a measurement of the mean hydrodynamic radius R_h. The fit of the autocorrelation function by the second cumulant function was performed by employing the MATLAB programme for Windows. Each result was an average of 10 or 15 measurements.

In the analysis of static light scattering measurements, the Rayleigh ratio for benzene was calculated to be $R_\theta = 0.136 \times 10^{-4}$ cm^{-2}. The refractive index of the buffer solution n_0 and the specific refractive index increment dn/dc for the three melanin solutions were measured. We obtained $n_0 = 1.3346$ and the optical constants K employed in Zimm plots (Eq. (1)) were evaluated: K(sepio-m.) $= 4.96 \times 10^{-8}$ g cm^{-2}, K(autoox.-m.) $= 6.44 \times 10^{-8}$ g cm^{-2} and K(enz.pol.-m.) $= 6.15 \times 10^{-8}$ g cm^{-2}.

For the angular range explored, $0.002 \leq q \leq 0.025$ nm^{-1}, the condition necessary to apply the fractal analysis to the system ($1/R_g \leq q \leq 1/r_o$) is satisfied for the average size of the individual particles (~ 15 Å, as shown in Section 1) and for the measured dimensions of the aggregates.

4. Results

4.1. Hydrodynamic characterization of the granules

4.1.1. Synthetic melanin by autooxidation

The process of formation of the granules of synthetic melanin during the autooxidative pathway in a salt free solution at pH 8 is shown in Fig. 1 (full circles) where the temporal behaviour of the hydrodynamic radius R_h, as deduced from the measurement of the apparent diffusion coefficient (Eq. (5)) for the particles in formation, is displayed.

If analyzed with a higher resolution, as is shown in the enlargement (Fig. 1, inset), the curve shows a behaviour described by large quasi-periodic fluctuations, even though the average value of R_h gradually increases with time.

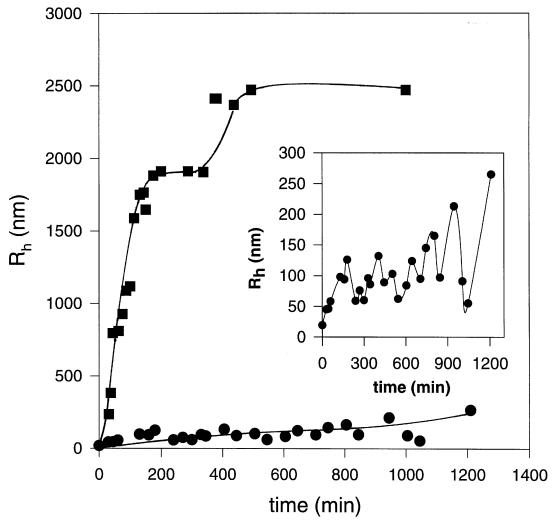

Fig. 1. Time course of aggregation kinetics of synthetic melanins. Hydrodynamic radius R_h is plotted vs. time: (●) L-Dopa autooxidation ([L-Dopa] $= 0.58 \times 10^{-3}$ g ml^{-1}) in borate buffer (pH 8, 0.1 M); (■) enzymatic (Tyrosinase) L-Dopa polymerization ([L-Dopa] $= 1.8 \times 10^{-6}$ g ml^{-1}, [Tyrosinase] = 8 mg/100 ml of saturated solution of L-Dopa) in borate buffer (pH 7, 0.1 M). Inset: magnification of the autooxidation process (the line is a guide for the eyes).

The final average dimension attained by the granules, measured on the solution stirred in air for a week, is $R_h = 263$ nm. This value has been assumed as final even though the aggregation process probably exceeds this limit to some extent.

As concerns the shape and size of a polyampholite macromolecule such as melanin, they critically depend on the environmental properties of the solvent, i.e. ionic strength and pH. By changing pH and ionic strength of the medium, the hydrodynamic radius measured changes as well. Fig. 2 is the plot of the reciprocal of the correlation time Γ, estimated from the first coefficient of the polynomial fit (Eq. (7)), vs. q^2 for the samples polymerized at different initial pHs. The average values of the hydrodynamic radii were estimated as follows: R_h (pH 7) = 610 nm, R_h (pH 8) = 263 nm, R_h (pH 9) = 69 nm, R_h (pH 10) = 31 nm. Fig. 3 displays the decrease in the average hydrody-

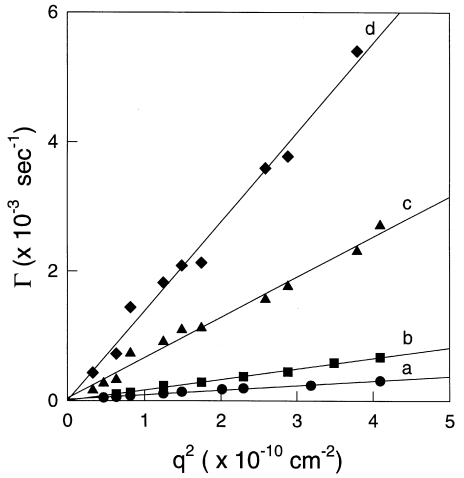

Fig. 2. Dependence of the initial slope of the correlation function on the square of the modulus of the scattering vector q^2 for melanin polymerized by autooxidation of L-Dopa ([L-Dopa] = 0.58×10^{-3} g ml^{-1}) in buffered solution (borate buffer) at different pHs: curve a, pH 7; curve b, pH 8; curve c, pH 9; curve d, pH 10.

namic radius measured for particles polymerized in solutions at increasing pH.

However, by increasing the ionic strength of the bath at fixed pH (pH 8) the dimensions of the granules increase as well; this behaviour is shown in Fig. 4.

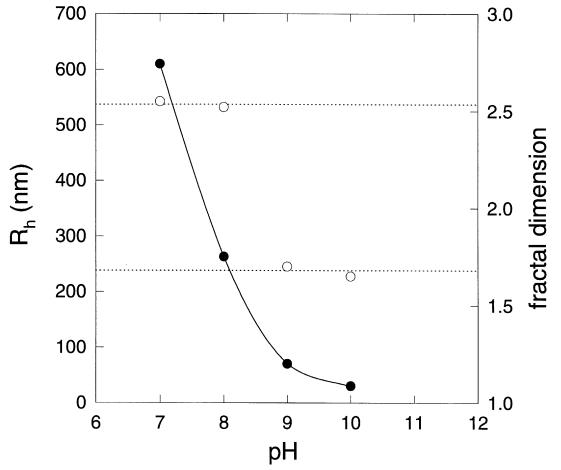

Fig. 3. pH dependence of the hydrodynamic radius R_h (●, scale on the left) and of the fractal dimension (○, scale on the right) of autooxidative L-Dopa melanin synthesized in borate buffer (0.1 M) at different pHs ([L-Dopa] = 0.58×10^{-3} g ml^{-1}).

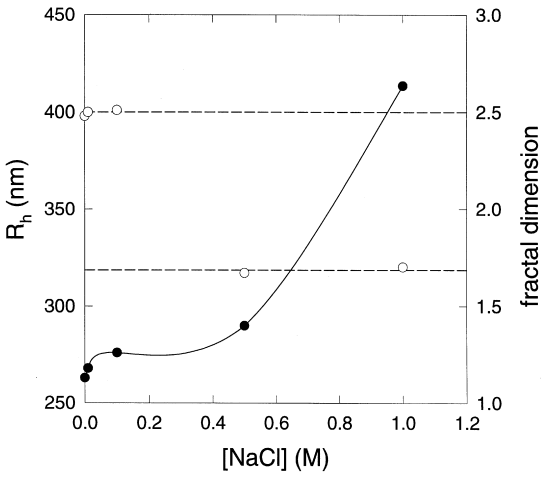

Fig. 4. Dependence of the hydrodynamic radius R_h (●, scale on the left) and of the fractal dimension (○, scale on the right) on the salt concentration [NaCl] of the medium of autooxidative L-Dopa melanin synthesized in buffered solutions (borate buffer at pH 8), ([L-Dopa] = 0.58×10^{-3} g ml^{-1}).

To investigate dimension and molecular weight of the granules obtained, the static light scattering intensity values measured on the solution polymerized at pH 8 were plotted following Zimm (Fig. 5). The parameters extracted, i.e. $\langle R_g^2 \rangle^{1/2}$ and $\langle MW \rangle$, are listed in Table 1, and the value of the mean hydrodynamic radius from DLS measurements is given in the third column.

The fourth column shows the calculated ratio $\langle R_g^2 \rangle^{1/2}/R_h$, which provides an indication on the shape of the polymer, the theoretical value for a sphere being 0.775 [22]. The data suggest a spherical symmetry for this synthetic autooxidative polymer.

4.1.2. Synthetic melanin by enzymatic polymerization

The time course of the enzymatic polymerization of L-Dopa melanin (Fig. 1, squared symbols) shows a very different behaviour from the spontaneous polymerization process as described above. The kinetics of growth of the enzymatically synthesized melanin is characterized by a double step line, the first plateau being formed 2.5 h after the start of the experiment: it leads to particles of average $R_h \sim 2 \times 10^3$ nm. The second stage of the process can be considered concluded in 6 to 8 h and corresponds to R_hs in the range 2.3×10^3

Table 1
Physical parameters characterizing melanin granules

Sample	$\langle MW \rangle$[a]	$\langle R_g^2 \rangle^{1/2}$ (nm)[a]	R_h (nm)[b]	$\langle R_g^2 \rangle^{1/2}/R_h$
Sepia melanin	7.4×10^6	90	101	0.891
Autoxidative melanin	7.7×10^7	191	263	0.726
Enzymatically polymerized melanin	6.6×10^9	312	2500	0.125

[a] From Zimm plot.
[b] From DLS measurements.

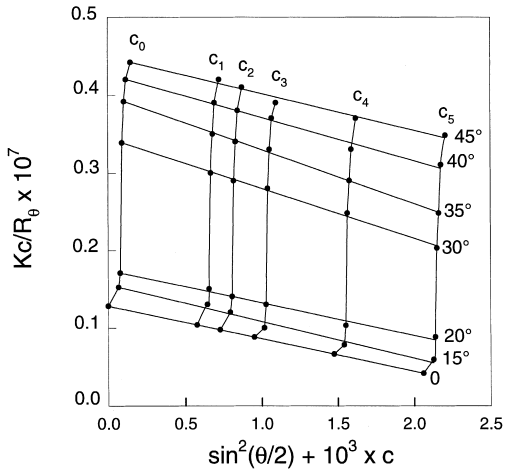

Fig. 5. Zimm plot of melanin polymerized by L-Dopa autooxidation ([L-Dopa] = 0.58×10^{-3} g ml^{-1}) in borate buffer (pH 8, 0.1 M). c_{1-5} refer to the melanin concentrations in buffer of the solutions employed: $c_1 = 0.58 \times 10^{-3}$ g ml^{-1}, $c_2 = 0.72 \times 10^{-3}$ g ml^{-1}, $c_3 = 0.95 \times 10^{-3}$ g ml^{-1}, $c_4 = 1.47 \times 10^{-3}$ g ml^{-1}, $c_5 = 2.06 \times 10^{-3}$ g ml^{-1}.

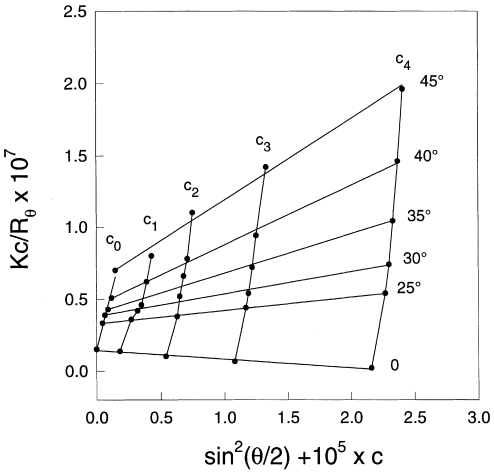

Fig. 6. Zimm plot of melanin polymerized by enzymatic oxidation ([L-Dopa] = 1.8×10^{-6} g ml^{-1}, [Tyrosinase] = 8 mg/100 ml of saturated solution of L-Dopa) in borate buffer (pH 7, 0.1 M). c_{1-4} refer to the melanin concentrations in buffer of the solutions employed: $c_1 = 1.8 \times 10^{-6}$ g ml^{-1}, $c_2 = 5.4 \times 10^{-6}$ g ml^{-1}, $c_3 = 10.8 \times 10^{-6}$ g ml^{-1}, $c_4 = 21.6 \times 10^{-6}$ g ml^{-1}.

to 2.5×10^3 nm. This behaviour is independent of the initial concentration of the precursor, and it was verified for different initial concentrations of L-Dopa, as previously described [23].

Fig. 6 displays the Zimm plot for this sample, and in Table 1 the calculated values $\langle R_g^2 \rangle^{1/2}$, $\langle MW \rangle$ and the ratio $\langle R_g^2 \rangle^{1/2}/R_h$ are listed.

For this enzymatically polymerized sample the data indicate a disproportionately large value of the hydrodynamic radius compared with the radius of gyration. This fact was explained by assuming a model at dishomogeneous density for the melanin granule, which could be described as a dense core surrounded by a branched, low density shell: such an object should be a powerful light scatterer at the level of the dense nucleus but at small angles the branches could also contribute to the scattered intensity and affect the hydrodynamic results. This picture, discussed in more detail in Section 5, could justify some controversial results such as the too large R_h value detected compared with that employed in the experiment and the angular range explored, and the deviation from the linearity of the Zimm plot at very low angles, i.e. in the region of the theoretical fitting, between $\theta = 15$ and $\theta = 0$.

For these reasons, the final R_h value measured is probably not a completely reliable numerical datum; however it has been quoted because of the peculiar physical situation reproducing.

4.1.3. Natural melanin from sepia inksac

The translational diffusion coefficient measured for the natural melanin examined, as extracted from the plot of the reciprocal of the correlation time vs. q^2 (Fig. 7), was $D = (2.13 \pm 0.24) \times 10^{-9}$ cm^2 s^{-1} for a sample obtained by dissolving melanin at concentration $c = 2 \times 10^{-4}$ g ml^{-1} in buffer at pH 8 and filtering after dilution with 0.5 μm millipore. The corresponding Stokes radius was calculated as $R_h = 101$ nm. By changing the concentration of the solution, the diffusion coefficient measured also changes. The extrapolation to zero melanin concentration of the linear correlation between the measured D vs. c (c ranged between 0.66 and 2×10^{-4} g ml^{-1}) allowed us to detect the theoretical D_0 value, $D_0 = 1.64 \times 10^{-9}$ cm^2 s^{-1} (Fig. 7, inset), from which the hydrodynamic radius value $R_0 =$ 130 nm was extracted.

The relatively high control of the degree of aggregation, by the filtration procedure, as well as the quality of the preparation of the natural sample, allowed us to obtain a more 'regular' Zimm plot (Fig. 8) than those obtained for the two synthetic melanins.

The $\langle R_g^2 \rangle^{1/2}$ and $\langle MW \rangle$ values extracted are listed in Table 1. In analogy with the synthetic

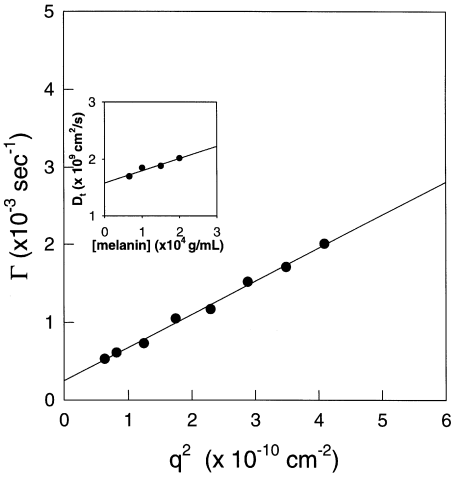

Fig. 7. Reciprocal of the decay time of the correlation function plotted as a function of q^2 for sepio melanin in 0.1 M borate buffer, pH 8. Inset: extrapolation to zero melanin concentration of the translational diffusion coefficient D.

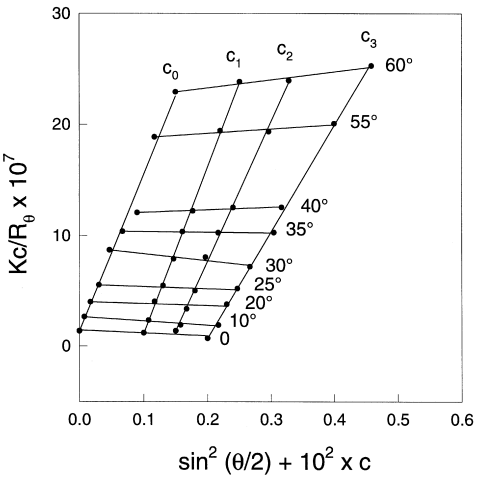

Fig. 8. Zimm plot for sepia-inksac melanin. c_{1-3} refer to the melanin concentrations in buffer of the solutions employed: $c_1 = 2 \times 10^{-4}$ g ml^{-1}, $c_2 = 1.5 \times 10^{-4}$ g ml^{-1}, $c_3 = 1.0 \times 10^{-4}$ g ml^{-1}.

samples the ratio $\langle R_g^2 \rangle^{1/2}/R_h$ was calculated by assuming for R_h the value obtained on the solution showing an O.D.(340 nm) comparable to that concerning the synthetic samples, i.e. the solution at $c = 2 \times 10^{-4}$ g ml^{-1}. The $\langle R_g^2 \rangle^{1/2}/R_h$ ratio calculated by means of the extrapolated value of the hydrodynamic radius R_0 further confirms the result obtained with the actual value employed, stressing even more the hypothesis for a spherical symmetry of the granule's shape.

4.2. Fractal analysis

The increase in the characteristic granule sizes with time for the two synthetic samples displayed in Fig. 1 can be fitted for the first 180 min by means of a power law, $R \sim t^C$, where $C = 1/d$, as expected for the growth of a fractal object such as colloid particles [24]. We obtained $d = 2.28$ for autooxidative melanin and $d = 1.65$ for the enzymatically polymerized sample. These values, in the range typical for the two aggregation kinetics regimes for fractals RLA and DLA respectively, as described in Section 1, directed the research study toward fractal analysis.

The $\ln(I)$ vs. $\ln(q)$ plots for natural and synthetic melanins, the autooxidative ones being pre-

pared in solutions at different initial pH, are shown in Fig. 9. Fractal dimensions extracted from the slope of the lines concerning autooxidative melanin, change abruptly when the pH solution changes from 8 to 9, so that the samples prepared at pH 7 and 8 aggregate in granules characterized by a fractal dimension $d \sim 2.5$, near to the typical value for RLA; but when pH rises to 9 and 10 the clusters are characterized by $d \sim 1.7$, the DLA typical fractal dimension (Fig. 3, right hand ordinate, hollow symbols). Fig. 9, in addition, displays the fractal behaviour for enzymatically synthesized melanin and sepio-melanin: a straight line fitting yields $d \sim 1.8$ for the synthetic and $d \sim 2.4$ for the natural polymer, typical for RLA dynamics.

The presence of salt in the starting solution at pH 8 does not greatly influence the size and the fractal dimension of the granules up to [NaCl] $\leq$ 0.5 M as Fig. 4 (right hand ordinate scale, hollow symbols) shows, so that the fractal dimension of the aggregates appears to range around the typical RLA value ($d \sim 2.5$); for increasing NaCl concentrations the fractal dimension changes at the DLA value, $d \sim 1.7$.

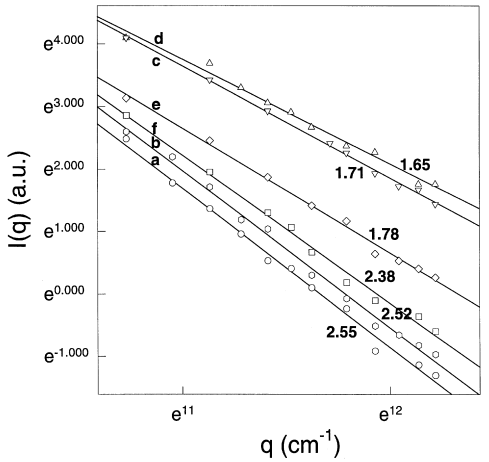

Fig. 9. A log-log plot of scattered light intensity $I(q)$ against q. The data refer to L-Dopa autooxidative melanin polymerized in salt free buffered (0.1 M borate buffer) solutions at pH 7 (a), pH 8 (b), pH 9 (c), pH 10 (d); enzymatically synthetized (e) and sepia melanin (f).

5. Discussion

The measurements performed to characterize the polymerization kinetics of the synthetic samples show very different behaviour in the time evolution of the average dimensions of the granules in solution during the two pathways, autooxidative and enzymatic: the presence of the enzyme not only influences the speed of the process and the sizes of the final granules but also the polydispersity of the product of polymerization which, during the autooxidative run, displays an oscillatory increase in the average sizes of the granules, while during the enzymatically catalyzed one appears to grow more continuously, the process being broken only by the presence of an intermediate plateau. The behaviour of the enzyme-driven polymerization is still under study in our laboratory.

The polymerization processes lead to granules of final different dimensions and shape. By comparing the values of the parameters listed in Table 1, it appears that the best agreement with the spherical model is obtained for autooxidative melanin, which in this sense is more similar to the natural one, even though for the natural sample, $\langle MW \rangle$, $\langle R_g^2 \rangle^{1/2}$ and R_h are all lower than the corresponding ones for the synthetic polymer at the same intermediate pH. By comparing the intensity values extracted from the zero concentration line of the Zimm plots vs. q to the theoretical functions employing the particle scattering factor $P(\theta)$ for two standard shapes, such as compact sphere and gaussian coil, a further indication as to the shapes of the molecules was gained. Fig. 10 shows the fitting for each sample, (a) for synthetic autooxidative, (b) for sepia and (c) for synthetic enzymatically polymerized melanin. The Gaussian coil model, taking into account a certain flexibility of the aggregates, was employed as indicative of the hypothesized floating structure of these branched polymers. The best agreement with both the models was obtained for autooxidative synthetic melanin and sepio-melanin, while enzymatically synthesized

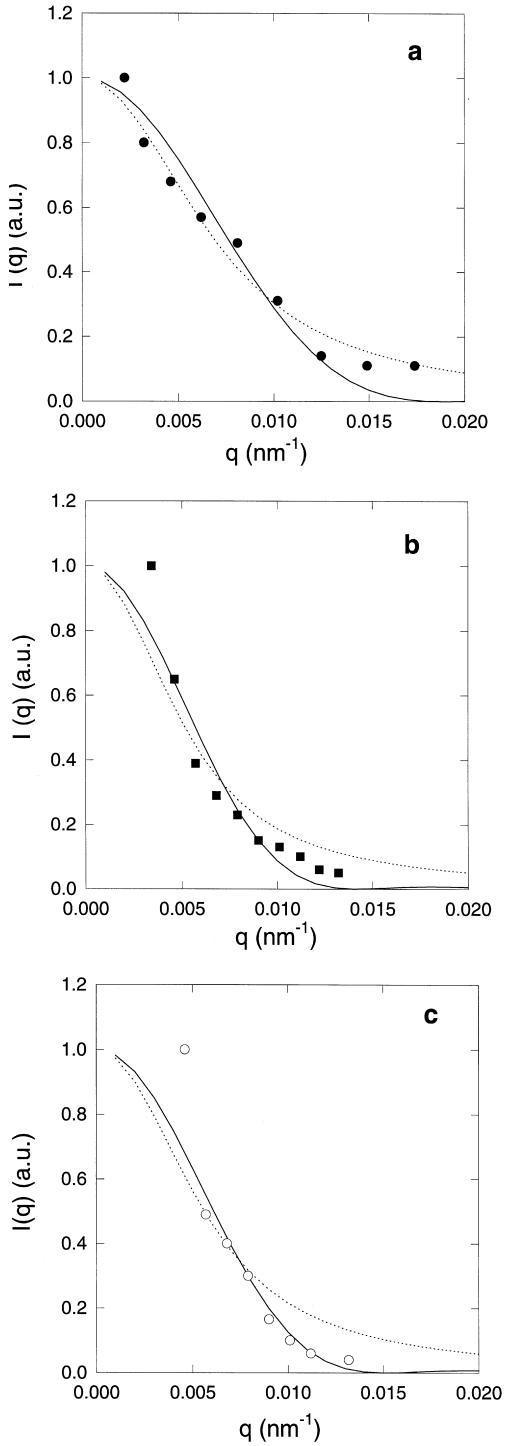

Fig. 10. Intensity of scattered light $I(q)$ vs. q for (a) synthetic autooxidative (●), (b) sepia (■), and (c) synthetic enzymatically polymerized (○) melanin: the solid line (——) shows the fitting obtained by employing the structure factor for a Gaussian coil, the dotted line (· · ·) for a solid sphere.

melanin displayed some deviations, in particular from the solid sphere model.

From this result it can be hypothesized that the direction of growth of the granules in the natural and synthetic autooxidative melanins is unimportant; the granules are probably obtained by addition of small units, the stiffness of the polymer probably being due to steric hindrance of the staked structure built by the conjugated indolic units, recognized by X-ray diffraction measurements [9,10,25]. The agreement recorded with the random coil model could account for the open texture of the branched structure of the aggregates. The $\langle R_g^2 \rangle^{1/2}/R_h$ values obtained confirm this picture.

The enzymatically polymerized sample deviates from this description. In fact the much larger R_h value of the granules than their $\langle R_g^2 \rangle^{1/2}$ value, and the biphasic polymerization kinetics recorded, both suggest the application of a model of aggregate at non-uniform density to the enzymatically polymerized melanin. Very low $\langle R_g^2 \rangle^{1/2}/R_h$ rates in branched polymers are indicative of unhomogeneous density in the clusters [26] which can be described by a denser core surrounded by a more tenuous structure branched and frequently highly hydrated. High hydration levels may be one of the causes contributing to deviation in the macromolecular shape from spherical symmetry. Following Tanford [27], a measure of the hydration of macromolecules or macromolecular assemblies can be obtained from the ratio R_h/R_S, R_S being the equivalent spherical radius, where $\bar{v}_p$ is the partial specific volume, and N_A Avogadro's number.

$$R_S = \left[\frac{3\bar{v}_p \langle MW \rangle}{4\pi N_A} \right]^{1/3} \tag{8}$$

The ratio R_h/R_S may be greater than unity for largely hydrated spherical particles,

$$\frac{R_h}{R_S} = \left[\frac{\bar{v}_p + \delta\bar{v}_0}{\bar{v}_p} \right]^{1/3} \tag{9}$$

where the increment $\delta\bar{v}_0$ in ml g^{-1} accounts for the volume of the solvation shell; for pure water $\bar{v}_0 = 1$ ml g^{-1}.

By applying this kind of analysis to our samples

(the density values for synthetic and natural melanin were deduced from Ref. [28]) we estimated a very large average amount of water for the enzymatically polymerized sample, as expected, i.e. $\delta\bar{v}_0 = 5.37$ ml g^{-1}. This value is indicative of both the effects sharing the deviation from the ideal spherical model: hydration and shape asymmetry. Natural and synthetic autooxidative polymers showed lower values ($\delta\bar{v}_0 \sim 1.2$ ml g^{-1}), and the result once again emphasizes the spherical symmetry of these aggregates.

Fractal analysis of the products of the aggregation processes allowed us to infer some hypotheses about the nature of the driving forces leading to the building of such different particles and to attempt to state a 'universal' physical parameter characterizing them. The power law linking the scattering intensity $I(q)$ with the wavevector q confirms the fractal nature of the aggregates of melanin, both natural and synthetic, the dynamic of aggregation being in agreement alternately with the RLA and DLA regimes depending on the chemical condition of the surroundings.

Synthetic autooxidative melanin polymerized in salt free bath, up to pH 8 appears to be formed by aggregates well described by the slow regime of aggregation RLA, but for polymerization at pH ≥ 9 we measured d typical for diffusion limited aggregation. This strong dependence of the d parameter on the pH can be related to the presence of electrical charges on the constituting units of the granule, so that the kinetic behaviour in the two regimes could be explained by the electrostatic interactions between the approaching particles, and in this sense the aggregation of aqueous gold colloids [24] is a very good model.

In the low pH region explored (pH 7–8) the aggregation proceeds at a low rate, the sticking monomers having the possibility to explore a large number of possible sticking sites. This approach leads to a deep interpenetration and therefore to dense aggregates ($d \sim 2.5$). At higher pHs, the presence of a net negative charge on the polymer gives rise to an interparticle Coulombic repulsive barrier, shifting the equilibrium in the solution toward dissociation: the aggregates structure as more tenuous and soft frames, the interior of the clusters being screened from penetration ($d \sim 1.7$).

The aggregation conditions can be controlled by the addition of NaCl in solution which acts by counterbalancing the charges on the granule surface, as the R_h vs. [NaCl] picture shows (Fig. 4, full symbols) for the melanin sample prepared at pH 8. The aggregation process appears to be strictly dependent on the [salt]/[melanin] rate in the solution. For our samples, aggregates maintain a fractal dimension typical of the RLA regime up to [NaCl] ≤ 0.5 M, but for larger salt amounts the screening of the surface charges is sufficient to induce the swelling of clusters up to $d \sim 1.7$ (Fig. 4, hollow symbols).

The natural sample examined shows a fractal dimension characteristic of the RLA regime, revealing a compact and dense structure.

As concerns the synthetic melanin by enzymatic oxidation, the fractal dimension detected ($d = 1.80$) could account for the branched and hydrated structure hypothesized.

6. Conclusions

In contrast with the continuous progress being made in the chemical investigation of the structure of melanin, physical studies have not led, up to now, to a consistent view of the physical parameters characterizing this biopolymer. The obstacles to successful physical studies have been twofold. First, various methods of preparation of synthetic melanin and of isolation of the natural ones undoubtedly produce samples having different physical properties. Second, it appears that none of the traditional methods of molecular weight and shape determination are adequate for the present problem, owing to the scarce solubility of these compounds in all solvents polar or non-polar.

The present approach to the problem, ultimately focused on the investigation of the growing mechanism by which melanin accumulates in the body, is based on the possibility to produce synthetic pigments, as similar as possible to the natural ones, starting from the same precursors as in vivo. But the biosynthesis of melanin is a very

complex process, proceeding by steps so strictly interrelated that the effective formation of the granules of macroscopic dimension can follow several different pathways if the conditions of the medium change. At fixed solution constraints the final sizes of the aggregates, although widely dispersed, exhibit few critical values possibly related to different packaged macromolecular units and hydration levels.

The analysis of the hydrodynamic parameters applied to the polymerization of synthetic melanin under different conditions of pH and ionic strength, the comparison with the values obtained for natural melanin from sepia inksac and the detection of a fractal dimension for the melanin granules, dependent on the chemical conditions of the medium as well, have allowed us to outline the following observations:

1. natural melanin, studied in a quasi-physiological condition of pH, polymerizes and aggregates in particles of average molecular weight $\sim 10^6$ and a radius of gyration $R_g \sim 90$ nm, with a spherical symmetry and with an open, rigid and not largely hydrated texture;
2. synthetic melanin by autooxidation at physiological pH appears the more reliable structural model for the natural one;
3. the enzyme probably plays a crucial and complex role in the polymerization catalyzed by Tyrosinase: the process appears biphasic and having as a product large floating structures, at non-uniform density and largely hydrated;
4. both natural and synthetic melanins grow as fractal aggregates of small units, the natural pigment following the RL kinetic regime and the synthetic ones leading to the DLA or RLA kinetics, depending on the conditions of the medium.

The balance of the electrostatic interactions of the charged groups on the surfaces of the polymer, both mutual and with water molecules in the surrounding medium could be the driving force of the aggregation process.

The tendency to bind water of the different ionizable groups in the different charge states present on the polymer surface, varying according to the pH value of the solution, could explain not only the formation of diverse types of polymer, according to the aggregation kinetics, but also the particular property of melanin, as a fractal object, giving rise to aggregates of reversible dimension [29]. The modulation of the pK of the surface functional groups by changing pH links the electronic properties of melanin with the solution properties of the aqueous surroundings. TSDC (thermally stimulated depolarization currents) measurements [30] performed in the past in our laboratory on L-Dopa autooxidative melanin showed different water desorption curves with different dehydration characteristic times for samples prepared at pH 10 ($t = 198$ min) and for those precipitated at pH 2 ($t = 68$ min). In the light of the present work, we can interpret the result by supposing that the soft melanin polymers, synthesized at basic pH and aggregating following the DL regime, have a structure inglobing a large quantity of water, organized and coordinated in the internal cages and difficult to extract. In the polymer prepared at a lower pH, the structure of the granule is denser and probably largely hydrated at the surface, and water can thus easily be desorbed.

Water in melanins could therefore behave as a restructuring agent dependent on the ionic properties of the medium. This hypothesis could explain not only the differences recorded in the polymerization pathways but also the 'reversibility' of the aggregation process shifting the pH of the solution to the extreme values, as mentioned in Section 1. Titration measurements [31] assure that around pH 8 the carboxylic groups are all deprotonated as well as approximately half of the hydroxylic residues of the phenolic groups; the aminic groups are in the NH_3^+ form. We can hypothesize that during the transition from acidic to basic pH the electrostatic repulsion among similarly charged groups could induce the softening of the structure, which becomes considerably hydrated and may become so tenuous and weak as to be easy to break and to dissolve into small granules. When pH decreases towards acidic values the Coulombic repulsive barrier is displaced and the subsequent reorganization of the cluster structure results in the 'squeezing out' of the

water molecules and in the coalescence of many clusters to originate denser and larger particles.

Acknowledgements

The author is grateful to Prof. Raimondo Crippa and Prof. Arnaldo Vecli of the University of Parma for their valuable discussions and suggestions regarding the paper.

References

[1] R.A. Nicolaus, Melanins, Hermann, Paris, 1968.
[2] G.A. Swan, A. Waggot, J. Chem. Soc.(C) (1970) 1409.
[3] J.N. Rodriguez-Lopez, J. Tudela, R. Varon, F. Garcia-Canovas, Biochim. Biophys. Acta 1076 (1991) 379.
[4] G. Prota, Melanins and Melanogenesis, Academic Press, 1992.
[5] R.E. Boissy, Dermatol. Clin. 6 (1988) 161.
[6] L. Zeise, L.B. Murr, R.M. Chedekel, Pigm. Cell Res. 5 (1992) 132.
[7] S. Ito, Biochim. Biophys. Acta 883 (1986) 155.
[8] L. Zeise, R.B. Addison, M.R. Chedekel, Pigm. Cell Res. Suppl. 2 (1992) 48.
[9] J. Cheng, C.S. Moss, M. Eisner, Pigm. Cell Res. 7 (1994) 255.
[10] J. Cheng, C.S. Moss, M. Eisner, Pigm. Cell Res. 7 (1994) 263.
[11] S.E. Harding, Biophys. Chem. 55 (1995) 69.
[12] J.S. Huang, J. Sung, M. Eisner, S.C. Moss, J. Gallas, J. Chem. Phys. 90 (1989) 25.
[13] T.A. Witten, Jr., L.M. Sander, Phys. Rev. Lett. 47 (1981) 1400.
[14] K.S. Schmitz, Dynamic Light Scattering by Macromolecules, Academic Press, 1990.
[15] B.H. Zimm, J. Chem. Phys. 16 (1948) 1093.
[16] M. Kerker, The Scattering of Light, Academic Press, 1969.
[17] B.J. Berne, R. Pecora, Dynamic Light Scattering, J. Wiley, 1976.
[18] H.E. Stanley, N. Ostrowsky (Eds.), On Growth and Form, M. Nijhoff, 1986.
[19] R. Jullien, Cont. Phys. 28 (1987) 477.
[20] P.R. Crippa, V. Horak, G. Prota, P. Svoronos, L. Wolfram, in: A. Brossi (Ed.), The Alkaloids, vol. 36, Academic Press, 1989, p. 254.
[21] P. Podini, R. Coisson, S. Cattani, Eur. J. Phys. (E) 10 (1989) 52.
[22] H. Chapman, V. Morris, R.R. Selvendran, Carbohydr. Res. 165 (1987) 53.
[23] L. Brancaleon, M.G. Bridelli, S. Losi, A. Vecli, Med. Biol. Environ. 21 (1993) 547.
[24] D.A. Weitz, J.S. Huang, M.Y. Lin, J. Sung, Phys. Rev. Lett. 54 (1985) 1416.
[25] S.S. Chio, X-Ray Diffraction and ESR Studies on Amorphous Melanin, Ph.D Thesis, University of Houston, 1977.
[26] K. Huber, W. Burchard, L. Fetres, Macromolecules 17 (1984) 541.
[27] C. Tanford, Physical Chemistry of Macromolecules, J. Wiley, 1961.
[28] M.R. Chedekel, B.L. Murr, L. Zeise, Pigm. Cell Res. 5 (1992) 143.
[29] B.B. Fedorov, B.A. Fedorov, Biophysics 38 (1993) 629.
[30] M.G. Bridelli, R. Capelletti, P.R. Crippa, Bioelectrochem. Bioenerg. 8 (1981) 555.
[31] J.E. McGinnes, P.R. Crippa, D.S. Kirkpatrick, P. Proctor, Physiol. Chem. Phys. 11 (1973) 217.